

This is the **accepted version** of the journal article:

Sciortino, Giuseppe; Sanna, Daniele; Lubinu, Giuseppe; [et al.]. «Unveiling VIVO2+ Binding Modes to Human Serum Albumins by an Integrated Spectroscopic-Computational Approach». Chemistry, Vol. 26, Issue 49 (September 2020), p. 11316-11326. DOI 10.1002/chem.202001492

This version is available at <https://ddd.uab.cat/record/281916>

under the terms of the  **COPYRIGHT** license

Unveiling $V^{IV}O^{2+}$ binding modes to human serum albumins by an integrated spectroscopic-computational approach

Giuseppe Sciortino,^{*,[a,b]} Daniele Sanna,^{*,[c]} Giuseppe Lubinu,^[b] Jean-Didier Maréchal,^[a] and Eugenio Garribba^{*,[b]}

- [a] Dr. G. Sciortino, Prof. J.-D. Maréchal xxx Ref. 1 xxx Ref. 2 xxx Mie commenti/aggiunte xxx Parti da controllare
 Department de Química
 Universitat Autònoma de Barcelona
 08193 Cerdanyola del Vallés, Barcelona, Spain
 E-mail: giuseppe.sciortino@uab.cat
- [b] Prof. E. Garribba, Dr. G. Lubinu
 Dipartimento di Chimica e Farmacia
 Università di Sassari
 Via Vienna 2, I-07100 Sassari, Italy
 E-mail: garribba@uniss.it
- [c] Dr. D. Sanna
 Istituto di Chimica Biomolecolare
 Consiglio Nazionale delle Ricerche
 Trav. La Crucca 3, I-07040 Sassari, Italy
 E-mail: danielle.sanna@cnr.it

Supporting information and the ORCID identification number(s) for the author(s) of this article can be found under: <https://doi.org/10.1002/chem.xxxx>.

Abstract: Human serum albumin (HSA) is involved in the transport of metal ions and potential metallodrugs. Depending on the metal, several sites are available, among which *N*-terminal (NTS) and multi-metal binding site (MBS). Despite the large number of X-ray determinations for albumins, only one structure with Zn^{2+} is available. In this work, the binding to HSA of $V^{IV}O^{2+}$ ion was studied by an integrated approach based on spectroscopic and computational methods, which allowed to completely characterize the systems even in the absence of an X-ray analysis. The behaviour depends on the type of albumin, defatted (HSA^d) or fatted (HSA^f). With HSA^d 'primary' and 'secondary' sites were revealed, NTS with (His3, His9, Asp13, Asp255) and MBS with (His67, His247, Asp249, Asn99 or H_2O); with increasing the ratio $V^{IV}O^{2+}/HSA^d$, 'tertiary' sites, with one His-N and others donors (Asp/Glu-O or carbonyl-O) are populated. With HSA^f , fatty acids (FAs) cause a rotation of the domains I and II, which results in the formation of a dinuclear ferromagnetic adduct ($(V^{IV}O)_2(HSA^f)$ with a $\mu_{1,1}$ -Asp249 and the binding of His247, Glu102, Glu252 and His67 or Asn99. FAs hinder also the binding of $V^{IV}O^{2+}$ to the MBS.

Introduction

Human serum albumin (HSA) is the most abundant protein in the blood plasma. Together with human serum transferrin (hTf), it transports in the organism most of the essential metal ions and their compounds, among which metal based potential inorganic drugs.^[1] Moreover, HSA can bind toxic metals, fatty acids (FAs) and endogenous and exogenous ligands.^[2] Despite the large number of X-ray determinations (XRD) of human and animal albumin (around 100 in the Protein Data Bank, PDB), only one structure with a metal ion, Zn^{2+} , is available.^[3] The binding sites of certain essential (Zn^{2+} , Cu^{2+}) or toxic (Ni^{2+} , Cd^{2+}) metal ions have been identified, while less is known about the binding of other metal ions.^[4, 5, 6] HSA contains two main sites: the *N*-terminal site (NTS or ATCUN motif),^[4] and the multi-metal binding site (MBS or site A).^[7] The NTS is present in most of all the albumins with a histidine in the third position such as HSA, bovine (BSA) and rat (RSA) serum albumin and is the

preferential site for Cu^{2+} and Ni^{2+} ions with the coordination of the terminal amino- NH_2 , the deprotonated amide- N^- of residues 2 and 3 and imidazole- N of His3. The MBS is located at the interface of subdomains IA and IIA and is the primary site for Zn^{2+} and other bivalent ions,^[5] with the binding of His67, His247, Asn99 and Asp249. Furthermore, other two sites were identified: site B, where Cd^{2+} and also Co^{2+} are bound by one His and several carboxylate of Asp or Glu residues,^[6, 8, 9, 10] and Cys34 – the only free thiol of HSA not engaged in intramolecular disulfide bridges – that binds Au and Pt compounds with deprotonated -SH group.^[11, 12, 13]

The relationship between the binding of fatty acids (FAs) and some metal ions was suggested:^[5, 14, 15] it is proved that Zn^{2+} coordination to the MBS can be hindered by the binding of fatty acids at site FA2 (one of the sites with highest affinity for FAs) inducing a rotation of the subdomains where the MBS is located and separating the Zn^{2+} coordinating amino acids. Such conformational changes can influence the binding of other metal ions and, therefore, the transport properties of albumin.

Among the most promising metals with pharmacological applications, $V^{IV}O^{2+}$ has shown very interesting anti-diabetic and anti-tumoral properties.^[16] After oral or intravenous administration, these vanadium-containing potential drugs reach the bloodstream where $V^{IV}O^{2+}$ can be released, mainly at low drug concentrations found in the organism, and could interact – other than with hTf – with albumin. Therefore, the study of the binding of $V^{IV}O^{2+}$ with HSA assumes great importance since it could affect the transport of V complexes, and the amount and chemical form which reach the target organs.

In the literature several papers were published on the interaction of $V^{IV}O^{2+}$ with HSA in its two forms, with or without FAs fatty acids (here designed as HSA^f and HSA^d);^[17] some proposals were advanced about the sites involved in the metal binding, but the systems are far from being fully characterized. Chasteen and Francavilla measured the relative intensity of the EPR resonances of $V^{IV}O^{2+}$ aquaion and $V^{IV}O^{2+}$ -albumin adducts as a function of

$V^{IV}O^{2+}$ /albumin ratio; with this procedure, they determined the number of the binding sites and their respective binding constants, distinguishing one “strong” and at least five “weak” binding sites.^[17a] Subsequently, these sites were named VBS1 and VBS2, respectively.^{[17i], [18]} Some authors suggested the involvement of the NTS in the metal coordination,^[17i] while evidence based on competition studies between Zn^{2+} and $V^{IV}O^{2+}$ indicated that $V^{IV}O^{2+}$ has two types of binding sites and one of them may correspond to the MBS (VBS1).^[19] Moreover, EPR spectra recorded on an equimolar solution $V^{IV}O^{2+}/HSA^f$ suggested a triplet state ($S = 1$), due to the ferromagnetic interaction of two metal ions in a dinuclear adduct designed as $[V^{IV}O]_2(HSA)_D$, where D stands for dinuclear,^[17i] in contrast, when the ratio $V^{IV}O^{2+}/HSA^f$ was $\geq 2:1$, the EPR resonances were attributed to various “weak” sites in a multinuclear complex $[V^{IV}O]_M(HSA)_M$ with $S = 1/2$, with M means mononuclear, in which the $V^{IV}O^{2+}$ ions are not magnetically interacting and are bound to different regions of protein.^{[17i], [17a], [19]} On the basis of EPR intensity, Costa Pessoa and coworkers affirmed that most of the paramagnetic V centers were non-detectable even at $V^{IV}O^{2+}/HSA$ ratio of 4/1 and concluded that the revealed $V^{IV}O$ complexes are minor species in equilibrium with the dimer $[V^{IV}O]_2(HSA)_D$ and hydrolytic products of $V^{IV}O^{2+}$.^[19] However, these conclusions were drawn considering equivalent the behavior of HSA^d and HSA^f . Here, we will demonstrate that this latter statement is not correct and fatty and defatted HSA differ for their metal binding properties.

In the light of these data, several issues remain to be explained: i) the influence of the FAs fatty acids in the formation of the metal adducts; ii) the nature of the “strong” site (VBS1) and if this corresponds to the NTS or MBS; iii) the structure of the dinuclear adduct $[V^{IV}O]_2(HSA)_D$; iv) the vanadium coordination environment in the “weak” sites VBS2 in $[V^{IV}O]_M(HSA)_M$. In this paper, the systems $V^{IV}O^{2+}/HSA^d$ and $V^{IV}O^{2+}/HSA^f$ were studied to unveil these unclear points aspects and examined at a molecular level using an integrated spectroscopic and computational multiscale approach. EPR spectroscopy allows the recognition of the type of amino acid donors involved in the metal coordination (for example, His-N, Asp/Glu-COO, or carbonyl-CO, etc.) but not the specific residues nor the three-dimensional structure.^{[20] [21]} Computational methods represent a valuable complementary tool to predict the binding sites and provide with their three dimensional models. Specifically, Density Functional Theory (DFT), Molecular and Quantum Mechanics (MM and QM) based methodologies as well as Molecular Dynamics (MD) and pattern recognition analysis techniques can be used to address the main steps during the metal-protein recognition process.^[22]

The results allowed to fully characterize the behavior of the two systems and to clarify the number and properties of the vanadium binding sites, even in the absence of an XRD. They could provide for useful information about the transport of vanadium and vanadium compounds in the organism. Finally, this approach may be applied to other

systems formed by a metal ion and a protein, for which an XRD is not available.

Results and Discussion

$V^{IV}O^{2+}$ binding to defatted human serum albumin (HSA^d)

EPR spectra were recorded on the system $V^{IV}O^{2+}/HSA^d$ as a function of the molar ratio and pH. In these experiments HSA^d from Sigma-Aldrich with codes A1887 and A3782 were used. In Fig. 1 the spectra measured on an equimolar solution containing A1887 are shown; all the full spectra together with the simulations with the software WINEPR SimFonia^[23] to extract their spin Hamiltonian parameters are reported in Figs. S1-S4 of the SI. In contrast with what was previously reported by some of us on HSA containing FAs fatty acids,^[17i, 17h, 24] only the signals of mononuclear $V^{IV}O^{2+}$ complexes with $S = 1/2$ were detected. It can be observed the formation of one species at pH 5.35 (indicated with IV in Fig. 1) and three additional adducts at pH > 6.40 (I, II and III). The values of $|A_z|$ are $171.2 \times 10^{-4} \text{ cm}^{-1}$ for IV, $162.9 \times 10^{-4} \text{ cm}^{-1}$ for I, $166.4 \times 10^{-4} \text{ cm}^{-1}$ for II and $169.0 \times 10^{-4} \text{ cm}^{-1}$ for III. The spin Hamiltonian parameters are listed in Table S1 of the SI. The data can be explained postulating that at acidic pH – when histidines are still protonated and cannot interact with the metal ion – the equatorial coordination positions are occupied by O-donors, for example carboxylate groups of Asp and/or Glu residues, amidic groups of the backbone and Asn and/or Gln or H_2O (IV). An increase of pH causes a spectral change due to the binding of stronger donors such as His-N (I, II and III) and these adducts become predominant at pH = 7.40. The first two sites populated at physiological pH are I and II, with a slight preference for I (named here ‘primary’ site) with

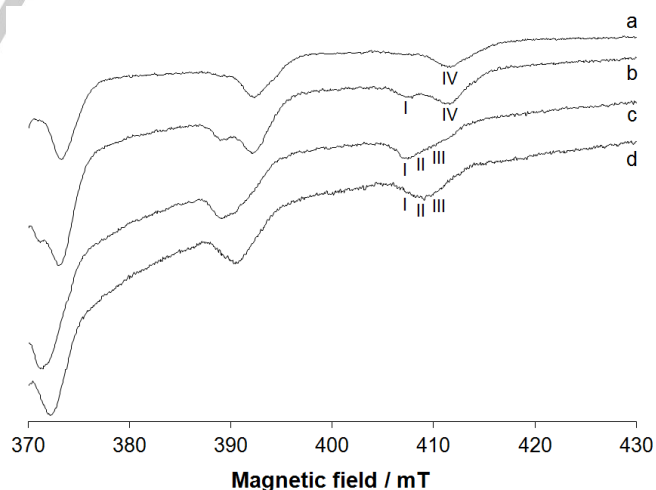


Figure 1. High field region of the X-band anisotropic EPR spectra recorded on frozen solutions (120 K) containing $V^{IV}O^{2+}/HSA^d$ at: a) ratio 1/1, pH 5.35; b) ratio 1/1, pH 6.40; c) ratio 1/1, pH 7.40 and d) ratio 4/1, pH 7.40. With I, II, III and IV the $M_I = 7/2$ resonances of the sites NTS, MBS, ‘tertiary’ (sites B) and ‘quaternary’ are indicated. $V^{IV}O^{2+}$ concentration was $7.5 \times 10^{-4} \text{ M}$ for the 1/1 ratio and $1.0 \times 10^{-3} \text{ M}$ for the 4/1 ratio. HSA^d used was a Sigma-Aldrich product with code A1887.

respect to II ('secondary' site). On the basis of the "additivity relationship", the empirical rule verified for a lot of $V^{IV}O$ complexes which allows estimating the ^{51}V hyperfine coupling (HFC) constant along the z axis (A_z^{estmtd}) from the sum of the contributions of each equatorial donor within $\sim 3 \times 10^{-4} \text{ cm}^{-1}$ from the experimental value,^[20] the A_z 's for I and II are compatible with two His-N plus a number of O-donors stemming from carboxylates (Asp and/or Glu residues), carbonyl or water. In contrast, for III, the weaker site or 'tertiary' site, the coordination of only one His is expected.

The relative strength of the two stronger binding sites I and II with respect to III was confirmed by the comparison of the EPR spectra at physiological pH recorded as a function of $V^{IV}O^{2+}/HSA^d$ ratio (Fig S5 of the SI): whereas the resonances I and II are detected when the spectrum is acquired at $V^{IV}O^{2+}/HSA^d$ 1/1 ratio, increasing the ratio up to 4/1 a broader band, composed by I and II plus the resonances of III, is observed (see also trace d of Fig. 1), suggesting that when I and II sites with two histidines bound to the metal are occupied, the additional $V^{IV}O^{2+}$ equivalents are distributed between the weaker 'tertiary' sites supposedly characterized by only one His and O-donors.

To get more information on the $V^{IV}O^{2+}$ binding sites location, EPR competition studies were carried out with Zn^{2+} and Ni^{2+} ions (Fig. 2). The full spectra are represented in Figs. S6-S12 of the SI. To interpret the data, it is necessary to premise that in the defatted human serum albumin the MBS is preserved and that zinc binds specifically to this site, while nickel to the NTS motif. The addition of one equivalent of Zn^{2+} to a solution containing $V^{IV}O^{2+}$ and HSA^d with a 1/1 molar ratio does not result in a

resonances for the sites I and II (trace b of Fig. 2), suggesting a slight competition between the two metals and that $V^{IV}O^{2+}$ remains bound to the 'primary' site I. Only increasing the $Zn^{2+}/V^{IV}O^{2+}$ ratio up to 2/1 and 4/1, appreciable changes were observed (traces c and d of Fig. 2). In contrast, the addition of one equivalent of Ni^{2+} is enough to remove from the 'primary' binding site $V^{IV}O^{2+}$ that remains bound to the sites II and III (trace e of Fig. 2), confirming the conclusions of Costa Pessoa and coworkers.^[19] To further validate this hypothesis, similar EPR experiments were performed using porcine serum albumin (PSA) that presents Tyr3 instead of His3 as the third residue of the polypeptide chain, making the NTS not available for the metal coordination and forcing the metal ions to bind to the MBS. The results on the system $V^{IV}O^{2+}/PSA$ allowed us to do a very important observation: the resonances I were lacking and only those indicated with II were revealed (trace f of Fig. 2). When one equivalent of zinc is added to this system (trace g of Fig. 2), Zn^{2+} is able to remove quantitatively $V^{IV}O^{2+}$ from binding site II, in contrast with the behavior of HSA^d for which there is no significant competition; in this system only the resonances of the weak site III are detected. These data, taken together, indicate that the 'primary' strong $V^{IV}O^{2+}$ binding site is located at the NTS of HSA^d (resonances indicated with I), while the 'secondary' site (II) could be found in the interdomain IA and IIA region and is identified with the MBS, both of the sites involving the coordination of at least two histidine side chains. Non-specific additional 'weak' binding sites, involving the coordination of one histidine and O-donors (resonances III), also exist in HSA^d . Finally, the resonances denoted with IV at pH < 6 can be attributed to the sites with coordination of only O-donors from Asp, Glu, Asn, Gln or from CO of the backbone.

Starting from the spectroscopic information, the interaction with $V^{IV}O^{2+}$ and HSA^d was examined with a multiscale computational approach: i) a complete model for the defatted albumin adding the last five N-terminal missing amino acids to the X-ray structure PDB 1A06 of the free HSA^d structure was generated; ii) the model was minimized and subsequently 100 ns of Molecular Dynamics (MD) were carried out to relax the new portion introduced (the RMSD plots of the trajectories were shown in Figs. S13 and S14 of the SI); iii) the MD trajectory was clustered and the representative structures of each pull of snapshots probed for zones in which at least two histidine residues featured α - and β -carbons within a range of distances from each queried grid point of 2.6-6.4 and 3.4-7.2 Å, respectively;^[25] iv) the models that satisfied these criteria were further evaluated with docking calculations;^[26] v) docking solutions were refined at full Quantum Mechanics (QM) level of theory and this step was followed by Density Functional Theory (DFT) simulations of the EPR HFC constants A_z that were compared with the experimental ones.

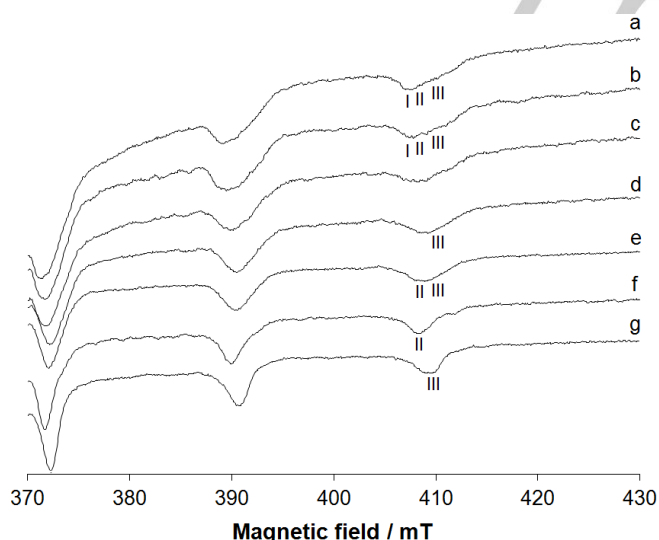


Figure 2. High field region of the X-band anisotropic EPR spectra recorded at pH 7.4 on frozen solutions (120 K) containing: a) $V^{IV}O^{2+}/HSA^d$ 1/1; b) $V^{IV}O^{2+}/Zn^{2+}/HSA^d$ 1/1/1; c) $V^{IV}O^{2+}/Zn^{2+}/HSA^d$ 1/2/1; d) $V^{IV}O^{2+}/Zn^{2+}/HSA^d$ 1/4/1; e) $V^{IV}O^{2+}/Ni^{2+}/HSA^d$ 1/1/1; f) $V^{IV}O^{2+}/PSA$ 1/1 and g) $V^{IV}O^{2+}/Zn^{2+}/PSA$ 1/1/1. With I, II and III the $M_I = 7/2$ resonances of the sites NTS, MBS and 'tertiary' (sites B) are indicated. $V^{IV}O^{2+}$ concentration was $7.5 \times 10^{-4} \text{ M}$ in all cases. HSA^d used was a Sigma-Aldrich product with code A1887.

significant change of the position and intensity of EPR

Table 1 'Primary' (NTS) and 'secondary' (MBS) binding sites of HSA^d for V^{IV}O²⁺ ion refined by QM methods, experimental, estimated and calculated A_z values, and electronic energies..

Site	Donors	V–N [a]	V–O [a]	V–OH ₂ [a]	A_z estmd [b,c]	A_z calcd [b,d]	$\Delta E_{\text{binding}}$ [e]
NTS- α	His3, His9, Asp13, Asp255	2.236, 2.199	1.975, 2.080	–	-165.0 [f]	-163.7 [d]	-31.7
NTS- β	His3, His9, Glu6; H ₂ O	2.126, 2.107	1.970	2.103	-168.8 [f]	-165.8 [d]	-18.4
NTS- γ	His3, His9, Asp13; H ₂ O	2.147, 2.150	1.995	2.071	-168.8 [f]	-170.4 [d]	-20.9
NTS- δ	His3, His9, His9-CO; H ₂ O	2.162, 2.111	2.097	2.046	-170.5 [f]	-175.3 [d]	-10.2
MBS ₁	His67, His247, Asp249; H ₂ O	2.108, 2.112	2.046	2.064	-168.8 [g]	-165.2 [e]	-26.2
MBS ₂	His67, His247, Asp249, Asn99-CO	2.135, 2.154	1.964, 2.034	–	-166.7 [g]	-169.5 [e]	-32.9

[a] Distance in Å. [b] A_z measured in 10^{-4} cm^{-1} units. [c] A_z estimated with the "additivity relationship". [d] A_z calculated with DFT methods. [e] $\Delta E_{\text{binding}}$ in kcal/mol. [f] Experimental value for the NTS site is $-162.9 \times 10^{-4} \text{ cm}^{-1}$. [g] Experimental value for the MBS site is $-166.4 \times 10^{-4} \text{ cm}^{-1}$.

Only two of the ten total clusters were found to have the necessary preorganization to bind the V^{IV}O²⁺ ion with at least two His side chains. The regions containing two potential N-donors were: the interdomain MBS involving His67 and His247 and the N-terminal site (NTS) with His6 and His9 side chains, that are sufficiently close to each other. Docking calculations were performed in these regions considering flexible histidines and neighboring residues (in a radius of 5 Å). Both δ and ϵ histidine tautomers were taken into account. Taking into account the EPR evidences the possibility to bind to the deprotonated ATCUN motif (NH₂, N⁻, N⁻, His3-N) has not been taken into account (*vide infra*). Preliminary dockings were performed activating all the four equatorial coordination positions in order to examine the case as general as possible. For the solutions with the metal binding from by three protein donors, the first coordination sphere was completed adding a water molecule and docking calculations were repeated to confirm the results using the moiety V^{IV}O(H₂O)²⁺, with three activated equatorial positions instead of the 'bare' V^{IV}O²⁺ as the ligand fragment for the protein.

In the N-terminal region four binding modes – named NTS- α , NTS- β , NTS- γ and NTS- δ – were identified with (His3-N, His9-N, Asp13-COO, Asp255-COO), (His3-N, His9-N, Asp13-COO; H₂O), (His3-N, His9-N, Glu6-COO; H₂O) and (His3-N, His9-N, His9-CO; H₂O) coordination, respectively (in Fig. 3 the structures obtained after the QM refinement are represented). The docking assay (summarized in Table S2 of the SI) suggests that NTS- α is the most stable binding mode with F_{max} and F_{mean} higher than 60 GoldScore units.

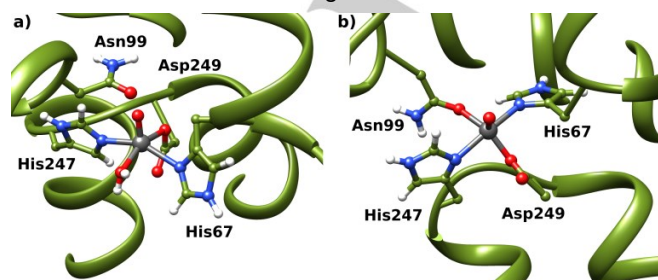


Figure 3 QM refined binding modes for V^{IV}O²⁺ ion at the N-terminal region of HSA^d: a) mode NTS- α ; b) mode NTS- β ; c) mode NTS- γ and d) mode NTS- δ .

The affinity of the modes NTS- β and NTS- γ results lower more than 10 GoldScore units compared to NTS- α , while the lowest scoring for the mode NTS- δ is coherent with the decrease in the donor strength replacing a carboxylate with a carbonyl donor.

Concerning the interdomain region, the results showed two potentials V^{IV}O²⁺ binding modes at the MBS site (indicated with MBS₁ and MBS₂ in Table 1) with the donor sets (His67-N, His247-N, Asp249-COO; H₂O) and (His67-N, His247-N, Asn99-CO, Asp249-COO) (Fig. 4 with the QM refined structures). In these adducts, the fourth equatorial position could be occupied by a water molecule or the amide oxygen of Asn99. To further validate the reliability of the docking approach and to discriminate between the four possible solutions at the NTS and two at the MBS region, the most stable docking solutions were refined by QM cluster method proposed by Siegbahn and Himo^[27] (structures represented in Figs. 3 and 4). The value of $\Delta E_{\text{binding}}$ for the sites NTS and MBS was calculated for reactions 1 and 2:

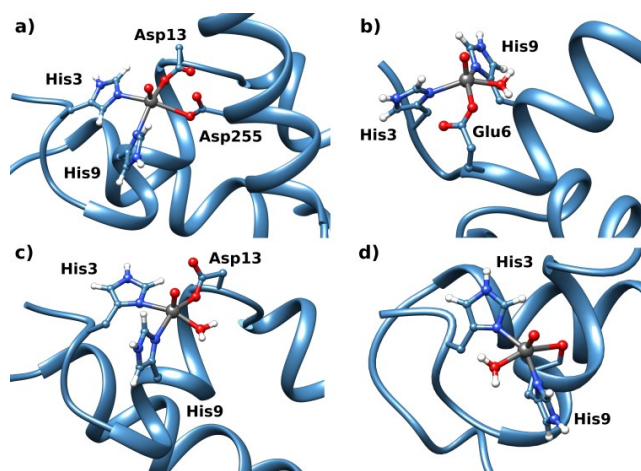
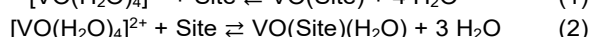
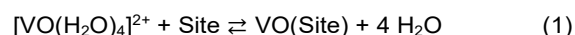


Figure 4 QM refined binding modes for V^{IV}O²⁺ ion at the MBS region of HSA^d: a) MBS₁ and b) MBS₂.

Table 2 'Tertiary' binding sites (sites B) of HSA^d and HSA^f for V^{IV}O²⁺ ion determined by docking methods.

Site	Residues	Coordination	V–N [a]	V–O [b]	<i>F</i> _{max} [c]	<i>F</i> _{mean} [d]
1	His367, Glu331; H ₂ O, H ₂ O [e]	N, CO; H ₂ O, H ₂ O	1.979	2.597	36.2	33.9
2	His510, Asp512; H ₂ O, H ₂ O [f]	N, COO; H ₂ O, H ₂ O	2.193	2.273	30.5	27.8
3	His338, Asp340; H ₂ O, H ₂ O [e]	N, COO; H ₂ O, H ₂ O	2.091	2.606	31.4	28.7
4	His535, Glu531, Asn503; H ₂ O	N, COO, CO; H ₂ O	2.282	2.169, 2.249	41.0	40.6
5	His288, Glu153; H ₂ O, H ₂ O [f]	N, COO; H ₂ O, H ₂ O	2.352	2.174	36.4	34.9
6	His128, Glu131; H ₂ O, H ₂ O [e]	N, COO; H ₂ O, H ₂ O	2.346	2.192	30.3	27.5

[a] Distance in Å. [b] Distance in Å (distance V–OH₂ not reported). [c] GoldScore *Fitness* value obtained for the more stable pose of each cluster (*F*_{max}). [d] Average value of GoldScore *Fitness* for each cluster (*F*_{mean}). [e] Water molecules *trans* to each other. [f] Water molecules *cis* to each other.

To exclude any bias of the docking simulations, in molecular dynamics (MD) the metal bond forces and equilibrium parameters were calculated for the solution at MBS₂, and the system submitted to additional 100 ns of MD to relax the structure and exclude that the low scoring could be originated from a non-correct starting orientation of the amino acid side chains.

The final values of $\Delta E_{\text{binding}}$ for the NTS are -31.7 kcal/mol (mode NTS- α), -18.4 kcal/mol (NTS- β), -20.9 kcal/mol (NTS- γ), -10.2 (NTS- δ), -26.2 kcal/mol (MBS₁) and -32.9 kcal/mol (MBS₂), see Table 1. The results are in good agreement with those based on pure scoring and population of GoldScore terms and indicate that in all the six cases $\Delta E_{\text{binding}}$ is negative. The order of binding energy is MBS₂ \approx NTS- α > MBS₁ >> NTS- γ \approx NTS- β > NTS- δ , which means that the binding modes MBS₂ and NTS- α will be preferred compared to other ones. QM refinement involve an improvement of the prediction of the angles and distances, which approach those expected for V–N(imidazole), V–O(carboxylate) and V–O(water) bonds (Table 1).^[28] Overall, the possible sites predicted resemble that of V-substituted carboxypeptidase, which has two His (one parallel and one perpendicular to V=O bond), one Glu and one H₂O and is characterized by $|A_z|$ of $165.9 \times 10^{-4} \text{ cm}^{-1}$,^[29] close to those experimentally measured for the resonances I (attributed to the NTS) and II (MBS).

Furthermore, the $|A_z|$ values for the NTS and MBS sites were calculated predicted by DFT methods – that today allow to predict the HFC constants for paramagnetic metals and vanadium in particular, with high accuracy^[30, 31] – and compared with the experimental ones (Table 1). Overall, these data and those for $\Delta E_{\text{binding}}$ suggest that in the N-terminal region the most stable site is NTS- α , while the two best options for MBS (MBS₁ and MBS₂) differ for the binding of CO group of Asn99 instead of a H₂O molecule and can be considered alternative. The HFC constants were also estimated with the "additivity relationship",^[20] using the contribution taken from ref.^[32] and the values of $|A_z|^{\text{estmtd}}$ confirm these predictions (Table 1).

To complete the description of the binding of V^{IV}O²⁺ to HSA^d, further docking calculations were carried out to find non-specific binding sites. Taking advantage by the recent paper by Handing *et al.*,^[3] regions able to coordinate Zn²⁺ with at least one His and one O-donor were probed for binding with the V^{IV}O(H₂O)²⁺/V^{IV}O(H₂O)₂²⁺ moieties.

As a result, the sites with the simultaneous coordination of (His367-N, Glu313-CO), (His510-N, Asp512-COO), (His338-N, Asp340-COO), (His535-N, Glu531-COO, Asn503-CO), (His288-N, Glu153-COO), and (His128-N, Glu131-COO) – the last two not found for Zn²⁺ ion^[3] – were predicted and these could be responsible of the resonances indicated with III in Figs. 1 and 2. The values of docking parameters for these adducts are reported in Table 2 and their structures in Fig. S15 of the SI. These sites are reasonable candidates to represent could correspond to those named B in the literature, with one His-N plus O-donors, which are the preferred by Co^{II} and Mn^{II} and are the second choice for Cd^{II}.^[5-6, 9-10, 15] On the basis of our results, it is important to note that B is not unique in the HSA^d but comprises a number of similar binding sites that share the same chemical features. Remembering that Chasteen and Francavilla found five "weak" binding sites for V^{IV}O²⁺ ion (named subsequently VBS2),^[17a] it is reasonable to argue that they coincide with the six sites found by dockings and listed in Table 2.

Finally, the adducts with coordination of only O-donors were examined. Among them, those with the coordination of three or two carboxylates, such as (Glu184, Asp187, Glu188) and (Glu97-COO, Glu100-COO), the same site found by Handing *et al.*^[3] for Zn²⁺, are worth being mentioned (Table S3 and Fig S16 of the SI). However, other sites with carboxylate groups exist on the protein surface and these could also form adducts with the V^{IV}O²⁺ ion. To these sites, named 'quaternary' and occupied before the deprotonation of histidine residues, can be attributed the EPR signals IV at pH < 6 (trace a of Fig. 1).

Overall, the results can be summarized as follows. At acid pH the V^{IV}O²⁺ ion occupies the 'quaternary' sites with the coordination of two or three Asp-COO and/or Glu-COO. When pH is around the neutrality, after the deprotonation of histidines, the binding mode changes and the 'primary', 'secondary' and 'tertiary' sites become available. The 'primary' and 'secondary' sites are observed at low V^{IV}O²⁺/HSA^d ratio (1/1) and correspond to the NTS with (His3, His9, Asp13, Asp255) coordination and MBS with (His67, His247, Asp249) plus the fourth binding of Asn99-CO or H₂O ligand. Notably, these two sites are the same as those determined by XRD for Zn²⁺^[3] with the difference that, for V^{IV}O²⁺ and Zn²⁺, the stability order is inverted. These correspond to the sites named 'strong' by

Chasteen,^[17a] and VBS1 by Costa-Pessoa.^[17] The NTS is in the highly disordered *N*-terminal region of the protein and was found for Zn^{2+} with equine serum albumin (ESA), while with HSA the anomalous signal observed during the X-ray diffraction study in proximity of His9 and Asp13 could indicate the possible presence of the metal.^[3] This explains why there is no competition between V and Zn at low molar ratio: in fact, the two metals occupy both the MBS (preferred by Zn^{2+}) and NTS (slightly preferred by $\text{V}^{\text{IV}}\text{O}^{2+}$), respectively. When the molar ratio $\text{V}^{\text{IV}}\text{O}^{2+}/\text{HSA}^{\text{d}}$ is increased, then the 'tertiary' sites – formed by one His-N and another donor, such as carboxylate or carbonyl – become populated (sites B). These are sites defined 'weak' by Chasteen^[17a] and VBS2 by Costa Pessoa.^[17]

It is noteworthy that $\text{V}^{\text{IV}}\text{O}^{2+}$, in contrast with Cu^{2+} and Ni^{2+} ion, does not interact with ATCUN motif since the donor set (Asp1-NH_2 , N^- , N^- , His3-N), where N^- denotes the deprotonated amide groups of residues 2 and 3, should give spin Hamiltonian parameters ($g_z = 1.960$ and $A_z = 153 \times 10^{-4} \text{ cm}^{-1}$ measured in the model system $\text{V}^{\text{IV}}\text{O}^{2+}$ –GlyGlyHis^[33]) significantly different from those experimentally measured for HSA. The "additivity relationship",^[20, 32] suggests $|A_z|^{\text{estmtd}}$ of $151.4 \times 10^{-4} \text{ cm}^{-1}$, very far from the values observed which are in the range $(163\text{--}169) \times 10^{-4} \text{ cm}^{-1}$. Moreover, to induce the deprotonation of amide nitrogens in the tripeptide GlyGlyHis and reveal the (NH_2 , N^- , N^- , His-N), coordination, a ligand-to-metal molar ratio of 15/1 must be used and this binding mode can be clearly detected only at $\text{pH} > 7.5$.^[33] Similar findings were also reached by other authors.^[17e]

To confirm the data obtained with HSA^{d} A1887, the experiments were repeated with albumin with code A3782. It shows the same complexation scheme with binding at physiological pH to the 'primary' and 'secondary' NTS and MBS plus, increasing the $\text{V}^{\text{IV}}\text{O}^{2+}/\text{HSA}^{\text{d}}$ ratio, the interaction with the 'tertiary' sites with only one His residue (Figs. S17 and S18 of the SI).

$\text{V}^{\text{IV}}\text{O}^{2+}$ binding to human serum albumin containing fatty acid (HSA^{f})

As reported in the literature, the level of medium- and long-chain FAs influence the binding of zinc and it was proposed that they act as a regulatory mechanism of its concentration. Among the seven sites were identified in HSA for medium- and long-chain FAs (from C10 to C18) named FA1–FA7 (plus two supplementary FA8 for short-chain FAs and F9, available at a saturating FAs concentration.^[10] Among them, the sites FA2, FA4 and FA5 exhibit the highest affinity.^[34] The binding of FAs to the site FA2, located at the interface of the subdomains IA and IIA, causes the rotation of these subdomains IA with respect to the subdomain IIA,^[35] and the fact that disruption of the site A MBS moving away the coordinating amino acids.^[1, 10, 10] Therefore, the site A or separating the coordinating amino acid of MBS that become is no longer available for Zn^{2+} or, in general, metal coordination after the binding of FAs.

High levels of FAs have been associated to an alteration of the zinc homeostasis and the consequent increase of free Zn^{2+} in the blood serum related to the neurodegeneration and cellular death, to an increased risk of thrombosis and to the development of various diseases, such as diabetes.^[37] The distribution of FAs between the binding sites of HSA depends on the FAs concentration in the blood and on their chain length and unsaturation degree. In normal conditions, 1 mol of human serum albumin transports from 0.1 to 2 mol of FAs fatty acids^[34] and only at elevated FAs concentrations more than 2 mol are bound to HSA and all the sites become occupied.^[15, 38] Taking into account that a significant fraction of FAs bind to FA4 and FA5 (i.e., those with the highest affinity together with FA2), part of the MBS could remain unaltered and interact with the metal ions even in presence of FAs. Therefore, studying both the forms of albumin appears to be fundamental to completely understand the binding and transport of the metal ions.

Some years ago, in the system $\text{V}^{\text{IV}}\text{O}^{2+}/\text{HSA}^{\text{f}}$ we reported the formation of a dinuclear species with spin state $S = 1$, $(\text{V}^{\text{IV}}\text{O})_2(\text{HSA}^{\text{f}})$ and several hypotheses on its structure were proposed.^[17f, 19] The signals of this adduct were revealed for $\text{V}^{\text{IV}}\text{O}^{2+}/\text{HSA}^{\text{f}}$ ratio < 2 and are covered at higher ratios by the greater intensity of the resonances of mononuclear species with $S = 1/2$ (Fig. S19 of the SI). The results obtained with HSA^{f} from Sigma-Aldrich with code A9511 were displayed also by HSA^{f} with code A1653, indicating that the presence of long chain FAs determines the different complexation scheme compared to HSA^{d} .

We decided to give insight on the nature of the dinuclear species using computational techniques. Several PDB structures of HSA crystallized in presence of FA with different chain length were analyzed, paying particular attention to the relative position of subdomains IA and IIA to find regions with at least two histidine residues able to coordinate a metal ion. This preliminary analysis show that: i) IA/IIA interdomain region does not present significant differences in the six structures analyzed from PDB (1E7I, 1E7F, 1E7E, 1BJ5, 1GNJ, 1GNI) and ii) the regions containing the His-N donors are the same as HSA^{d} , except for the MBS, where His247 and His67 are separated. Docking calculations were performed in the interface of subdomains IA and IIA of the XRD structure crystallized in presence of stearic acid (PDB 1E7I^[35a]), considering flexible the histidine side chains and neighboring residues (with a radius of 5 Å). The dinuclear structure prediction was carried out blindly docking a first $\text{V}^{\text{IV}}\text{O}^{2+}/\text{V}^{\text{IV}}\text{O}(\text{H}_2\text{O})^{2+}$ moiety on the IA and IIA interdomain region. This analysis suggested three possible binding modes. The first docking assay was followed by subsequent dockings of an additional $\text{V}^{\text{IV}}\text{O}^{2+}/\text{V}^{\text{IV}}\text{O}(\text{H}_2\text{O})^{2+}$ to the three structures individuated in the first step. As a result, four geometrically consistent dinuclear candidates were found (indicated with 1–4 in Table 3 and shown in Fig. 5). The dimers 1–4 were refined by full QM cluster method proposed by Siegbahn and Himo.^[27] In all of them, Asp249 acts as the bridge; for three structures the binding is $\mu_{1,1}$ and is supported by a $\mu\text{-OH}^-$ ion, while the fourth structure presents a $\mu_{1,3}$ behavior

Table 3. Structural and magnetic data for $(VO)_2^D(HSA)^f$ dinuclear species.

Dimer	J [a,b]	Magnetic coupling	$V \cdots V$ [c]
1	19.88	Ferromagnetic	3.164
2	6.99	Ferromagnetic	3.173
3	0.13	Ferromagnetic	4.876
4	-25.42	Antiferromagnetic	3.255

[a] J value in cm^{-1} . [b] J determined with the method reported in refs. [39]. [c] Distance between V atoms in Å.

of Asp249. This site agrees well with the considerations proposed by Costa-Pessoa and co-workers, who suggested that Glu252 might be involved in V coordination.^[19] In all the structures Glu100, His247, and Glu252 take part to the coordination, to which Asn99 may add; His67 binds V in the dimers 1, 3 and 4 but not in 2.

The predicted models could rationalize the formation of $(V^{IV}O)_2^D(HSA)^f$ in the system with FAs fatty acids bound to HSA, in which the mutual rotation of the subdomains IA and IIA results in a separation of His247 and Asp249 residues from His67 and Asn99 – involved in the formation of the mononuclear adduct with HSA^d – by 4–6 Å,^[5, 7, 36a] which favors the accommodation of two $V^{IV}O^{2+}$ ions and formation of the bridge represented by Asp249 (Fig. 5). The exchange coupling constant J was calculated to determine the nature of the magnetic interaction between the two unpaired electrons on V^{IV} , ferro- or antiferromagnetic. The results show that for three dinuclear structures (1–3 in Table 3) the coupling is ferromagnetic, in agreement with EPR data that suggest a triplet state; in contrast, for the dimer 4 the interaction is antiferromagnetic and, for this reason, it can be excluded as a possible candidate for $(VO)_2^D(HSA)^f$.

The EPR spectrum of $(VO)_2^D(HSA)^f$ was simulated in this study with a zero-field splitting D of $605 \times 10^{-4} \text{ cm}^{-1}$ (649.8 Gauss) and $g_{x,y,z} = \{1.999, 1.999, 1.985\}$ and $A_{x,y,z} = \{45.0, 45.0, 80.0\} \times 10^{-4} \text{ cm}^{-1}$ (Fig. S20 of the SI). The HFC constant A_z is one half of the value which would be

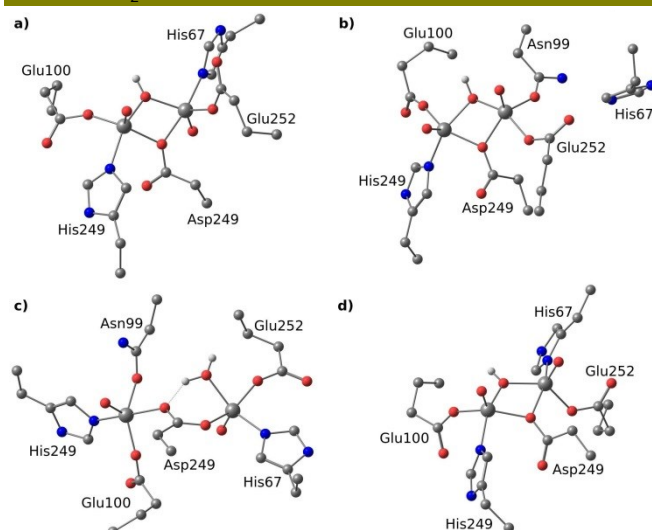


Figure 5. DFT optimized geometry of the dinuclear $V^{IV}O^{2+}$ adducts at MBS for HSA^f : a) dimer 1; b) dimer 2; c) dimer 3 and d) dimer 4. Hydrogen atoms and non-coordinating residues have been omitted for clarity.

observed for the mononuclear $V^{IV}O$ species with the same equatorial coordination mode.^[40] If D has contribution only from dipolar interaction, the approximate value of the distance R between the two V centers can be derived with eq. 1:^{[41], [42]}

$$D = \pi \frac{3}{2} \left(\frac{\mu_0}{4\pi} \right) \left(\frac{g^2 \beta^2}{R^3} \right) = 1.39 \times 10^4 \left(\frac{g}{R^3} \right) \quad (1)$$

where D is measured in Gauss and R in Å. For the experimental mean value of g , R is 3.49 Å, in line with the calculated value for dimers 1, 2 and 4 (even though this latter can be discarded because antiferromagnetic). Summarizing the data, the structure corresponding to the dimers 1 and 2 could be close to that formed under physiological conditions for the adduct $(VO)_2^D(HSA)^f$. The structure of dimer 1 bound to the MBS site of HSA^f is depicted in Figure 6.

When the ratio $V^{IV}O^{2+}/HSA^f$ is > 2 , the resonances attributable to sites with an only one $V^{IV}O^{2+}$ ion bound ($S = 1/2$) were revealed and these are superimposed to the low intensity absorptions of $(V^{IV}O)_2^D(HSA)^f$. When the spectra are recorded as a function of pH with molar ratio $V^{IV}O^{2+}/HSA^f = 4$, the 'quaternary' sites with only O-donors are observed at pH 5.00 (IV in Fig. S21 of the SI), while with increasing pH the 'primary' site NTS and the various 'ternary' sites with one His-N-donor are revealed (I and III). Interestingly, the resonances corresponding to the 'secondary' site MBS were not detected (Fig. S21 of the SI) due to the formation of the dimeric adduct $(V^{IV}O)_2^D(HSA)^f$. In these species, the binding to the metal of Cys34 with the –SH group can be excluded since – for the "additivity relationship" [20] – the value of A_z would be much smaller than those experimentally observed.

The effect of fatty acids on the complexation scheme of $V^{IV}O^{2+}$ was investigated also with HSA^f from Sigma-Aldrich with code A1653. Its behavior is identical as HSA^f with code A9511, confirming the results just discussed (Fig. S22 of the SI).

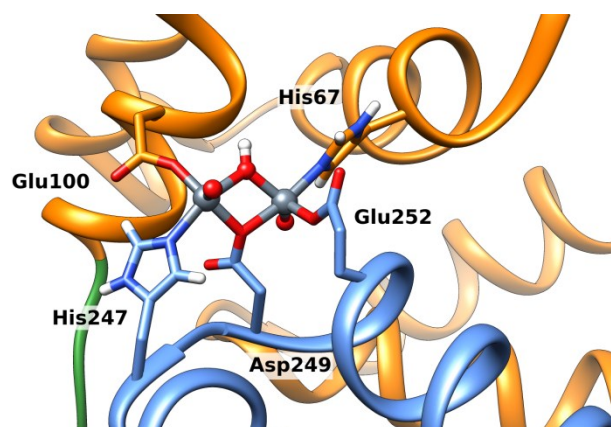


Figure 6. DFT refined geometry of the dinuclear 1 $V^{IV}O^{2+}$ at the MBS site of HSA^f . Subdomains IA and IIA are shown in blue and orange, respectively.

Conclusions

The study of the metal binding to proteins has a fundamental importance in biology, pharmacy and medicine. In fact, on one hand metal ions, in a free or complexed form, are part of the active site of proteins with several physiological functions (transport, storage, enzymatic, etc.), on the other metal compounds show pharmacological activity and are used or tested for the treatment of various diseases, such as ulcer, arthritis, diabetes and cancer. To characterize these systems, different instrumental techniques are available, but in most of cases – in the absence of X-ray determinations – the information is only partial and the exact location of the binding sites, the identity of the donors involved in the metal coordination and the complete three-dimensional description cannot be obtained. To overcome this limitation and complement the instrumental data, we developed a methodology to predict the coordination bond between a metal and a protein through dockings methods which can be subsequently refined with QM/MM or QM calculations.^[26] Human serum albumin (HSA) is, with transferrin, the most important protein of the blood serum involved in the transport of various essential and toxic metal ions and potential metallodrugs. Depending on the chemical properties of metals, several sites are available, among which the *N*-terminal site (NTS) – with which Cu^{2+} and Ni^{2+} interact – and the multi-metal binding site (MBS or site A), preferred by Zn^{2+} and Cd^{2+} , plus the not yet identified site B, the strongest for Co^{2+} and Mn^{2+} .^[19] The binding of $\text{V}^{\text{IV}}\text{O}^{2+}$ ion, which among the three oxidation states +III, +IV, +V revealed in biological systems, is the most stable form under physiological conditions and is probably released by antidiabetic and anticancer vanadium drugs, is still elusive and, for this reason, we applied an integrated approach based on EPR spectroscopy and docking/QM methods to study its interaction both with defatted (HSA^{d}) or fatted (HSA^{f}) albumin. On the whole, the behavior and the binding sites of $\text{V}^{\text{IV}}\text{O}^{2+}$ are very similar to Zn^{2+} , recently determined by an X-ray diffraction analysis.^[9]

For HSA^{d} , four types of sites were predicted: i) **NTS**. This is the 'primary' site in the *N*-terminal region with (His3, His9, Asp13, Asp255) coordination. ii) **MBS or site A**. The multi-metal binding site (MBS) is the 'secondary' site for $\text{V}^{\text{IV}}\text{O}^{2+}$ ion with (His67, His247, Asp249) coordination plus the weak binding of Asn99-CO or H_2O ligand. NTS and MBS have a comparable stability with a slight preference for the NTS and coincide with those named 'strong' by Chasteen^[17a] and VBS1 by Costa-Pessoa.^[17] iii) **Sites B**. The sites B are not specific and weaker than NTS and MBS, with one His-N and another O-donor such as Asp/Glu-O or carbonyl-O, populated with increasing the $\text{V}^{\text{IV}}\text{O}^{2+}$ /ratio; for the first time, the exact position of such sites and the amino acids involved in the interaction have been determined. These were proposed previously but not located^[5-6, 9-10, 15] and for $\text{V}^{\text{IV}}\text{O}^{2+}$ were named 'weak' by Chasteen^[17a] and VBS2 by Costa-Pessoa.^[17] iv) **Sites C**. These are 'quaternary' sites with only O-donors, stemming

from carboxylate of Asp or Glu, or from carbonyl groups of the backbone, and are occupied at acid pH. Following the nomenclature used in the literature, these could be named sites C.

The presence of **FAs fatty acids** in HSA^{f} results in a different behavior and this fact must be taken into account in the analysis of the transport of metal ions and metal compounds. **FAs Fatty acids** cause a rotation of the subdomains IA and IIA and the formation of $[\text{V}^{\text{IV}}\text{O}]_2^0(\text{HSA})$, which was revealed by EPR but never rationalized up to now,^[17f, 19] in which a $\mu_{1,1}$ -Asp249 bridges the two $\text{V}^{\text{IV}}\text{O}^{2+}$ ions with a ferromagnetic coupling. With HSA^{f} , the **FAs fatty acids** hinder the formation of mononuclear adducts at the MBS and, for this reason, influence the binding of metal ions that prefer this site (Zn^{2+} and Cd^{2+} beside $\text{V}^{\text{IV}}\text{O}^{2+}$), which are forced to move to the available 'primary', 'tertiary' and 'quaternary' sites.

Finally, we believe that the integrated approach presented here could be applied not only to characterize the $\text{V}^{\text{IV}}\text{O}^{2+}$ /HSA systems but also to determine the binding of other metal species to other proteins, integrating the best instrumental technique (for example, EPR for a paramagnetic and NMR for a diamagnetic ion) with docking/QM calculations. Therefore, with this approach complex systems such as (metal ion)–protein could be completely characterized even in the absence of an X-ray diffraction analysis.

Experimental Section

Chemicals. Water was deionized prior to use through the purification system Millipore MilliQ Academic. Metal solutions were prepared from $\text{VOSO}_4 \cdot 3\text{H}_2\text{O}$, $\text{ZnSO}_4 \cdot 7\text{H}_2\text{O}$ and $\text{NiSO}_4 \cdot 7\text{H}_2\text{O}$. Metal salts and 4-(2-hydroxyethyl)piperazine-1-ethanesulfonic acid (HEPES) were Sigma-Aldrich products of the highest grade available and used as received. Defatted and fatted human serum albumin were purchased from Sigma-Aldrich with codes A1887 and A3782 (HSA^{d}), A9511 and A1653 (HSA^{f}). Porcine serum albumin (PSA) was a Sigma-Aldrich product with code A1830.

EPR measurements. The solutions for EPR measurements were prepared by dissolving $\text{VOSO}_4 \cdot 3\text{H}_2\text{O}$ in ultra-pure water in order to get a $\text{V}^{\text{IV}}\text{O}^{2+}$ concentration in the range $(0.75\text{--}1.31) \times 10^{-3}$ M, depending on the ratio $\text{V}^{\text{IV}}\text{O}^{2+}$ /albumin. Argon was bubbled through the solutions to ensure the absence of oxygen and avoid the oxidation of $\text{V}^{\text{IV}}\text{O}^{2+}$ ion. To the solutions, HEPES buffer of 1.00×10^{-1} M concentration was added. The value of pH was kept around 4.0–4.5 to avoid hydrolysis and, to 1 mL of the solutions with the $\text{V}^{\text{IV}}\text{O}^{2+}$, PSA, HSA^{f} or HSA^{d} were added to obtain the desired $\text{V}^{\text{IV}}\text{O}^{2+}$ /albumin ratio. Subsequently pH was raised around 7.4 and EPR spectra were immediately recorded at 120 K with an X-band Bruker EMX spectrometer equipped with a HP 53150A microwave frequency counter. The microwave frequency was in the range 9.40–9.42 GHz, microwave power was 20 mW, time constant was 81.92 ms, modulation frequency 100 kHz, modulation amplitude 0.4–1.0 mT, resolution 4096 points. When the samples were transferred into the EPR tubes, the spectra were immediately

measured. Signal averaging was used to increase the signal to noise ratio.^[17]

The spectra were simulated (Figures S1-S4 and S20 of the SI) with the software WINEPR SimFonia.^[23]

DFT, MD and docking Calculations. The $V^{IV}O^{2+}$ ion, modeled as $[V^{IV}O(H_2O)_4]^{2+}$, and all the adducts were optimized with Gaussian 09 (revision D.01)^[43] at B3P86/6-311++g(d,p) level of theory using the SMD model^[44] for water. Frequency calculations were computed to ensure that the structure was a minimum in the potential energy surface.

The model of the defatted albumin were built with Modeller,^[45] adding the last five N-terminal missing amino acids to the X-ray structure 1AO6 of the unbound HSA^d. Molecular Dynamics (MD) simulations were set up with Xleap,^[46] which was instructed to solvate the protein with a cubic box of pre-equilibrated TIP3P water molecules and balance the total charge with Cl^- ions (ions94.lib library). The AMBER99SB force field^[47] was used for the standard residues, while V-bonding force constants and equilibrium parameters were obtained through the Seminario method, using the MCPB.py.^[48] During MDs solvent and the whole system were sequentially submitted to 3000 energy minimization steps, then, thermalization of water molecules and side chains was achieved by increasing the temperature from 100 K up to 300 K. MDs under periodic boundary conditions were carried out during 100 ns with OpenMM engine^[49] through OMMProtocol.^[50] Analysis of the trajectories was carried out by means of cpptraj implemented in ambertools16.^[46] The implemented clustering algorithm was used to generate ten clusters taking the RMSD between frames as distance metric. The representative structure of the most populated cluster was used in the further structural analysis in which each structure was probed for the zones with at least two potential coordinating residues (Asp, Glu, Asn, Gln and His) using multisite.py.^[25]

Docking calculations to the HSA^d were carried out through GOLD 5.8 software^[51] on the selected frames, while for the analysis of HSA^f the XRD structure of albumin crystallized in presence of steric acid (PDB 1E7I ^[35a]) was used. The PDB structure was cleaned removing all the small molecules and crystallographic waters, and hydrogen atoms were added with the UCSF Chimera program.^[52] The proteins were docked with $V^{IV}O^{2+}$, $V^{IV}O(H_2O)^{2+}$, and $V^{IV}O(H_2O)_2^{2+}$ moieties, obtained from the optimization of the aquaion $[V^{IV}O(H_2O)_4]^{2+}$. The equatorial positions were activated replacing the equatorial water(s) with dummy hydrogen atoms according to what was recently established.^[26, 53] All dockings were computed considering both the protonation states at δ and ϵ nitrogens of His imidazole ring. The docking simulations were carried out constructing in the region of interest an evaluation sphere of 12 and 5 Å for HSA^d and HSA^f respectively, taking into account side chains flexibility using the GOLD implemented rotamers libraries.^[54] Genetic algorithm (GA) parameters have been set to 50 GA runs and a minimum of 100,000 operations. The other parameters of GA were set to default. The solutions were analyzed by means of GaudiView.^[55]

The scoring (*Fitness* of GoldScore) was evaluated applying the modified version of GoldScore scoring function, which was validated in previously published papers.^[26, 53] The best solutions (binding poses) were evaluated through i) the mean (F_{mean}) and the highest value (F_{max}) of the scoring (*Fitness* of GoldScore)

associated with each pose and ii) the population of the cluster containing the best pose.

The refinement of the $V^{IV}O^{2+}$ -HSA^d and $V^{IV}O^{2+}$ -HSA^f adducts found by dockings was performed cutting out the region with the $V^{IV}O^{2+}$ ion, and neighbor interacting amino acid side chains and freezing the backbone atoms as reported by Siegbahn and Himo.^[27] The resulting clusters contain 90 (site NTS- α), 70 (NTS- β), 45 (NTS- γ), 49 (NTS- δ), 57 (MBS1) and 54 (MBS2) atoms, and 101, 118, 101 119 atoms for the dimers **1-4**. The geometry relaxation and ΔE calculations were performed at B3P86/6-311++g(d,p) level of theory within the framework of SMD model^[44] for water.

The details of the docking protocol, the atoms parameter libraries for $V^{IV}O^{2+}$ atom type, the vanadium "coordination" energetic terms implemented in the GoldScore scoring function, examples of input and output GOLD files, the force constants for vanadium and equilibrium parameters derived with Seminario methods, and – finally – Cartesian coordinates of the DFT optimized structures represented in Figures 3-5 are provided in the SI.

The prediction of the ^{51}V HFC constants (A) was performed Gaussian 09 (revision D.01)^[43] on the optimized structures at BHandHLYP/6-311+g(d) level of theory, according to the procedures previously published.^[56] The theory background can be found by the interested readers in refs. ^[31]. The exchange coupling constant J for the dinuclear adduct $[VO_2]_2P(HSA)$ was calculated with the functional B3LYP and 6-311g basis set with the software ORCA,^[57] according to the method reported in the literature.^[58] Using $S_1 = S_1 = 1/2$ in the Heisenberg Hamiltonian $\hat{H} = -J\hat{S}_1 \cdot \hat{S}_2$ the value of J can be expressed as: $J = E_{BS} - E_{HS}$, where E_{BS} and E_{HS} are the energies of the broken-symmetry solution and triplet state.

Acknowledgements

E.G., G.S., D.S., and G.L. thank Regione Autonoma della Sardegna (grant RASSR79857) and Università di Sassari (fondo di Ateneo per la ricerca 2019) for financial support. G.S. and J.-D.M. thank also Spanish MINECO (grant CTQ2017-87889-P) and Generalitat de Catalunya (2017SGR1323).

Conflicy of interest

The authors declare no conflict of interest.

Keywords: oxidovanadium(IV) ion • human serum albumin • fatty acids • docking and QM calculations • Electron Paramagnetic Resonance

References Controllare abbrev.

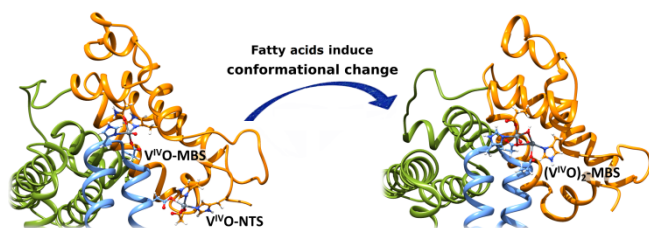
- [1] W. Bal, M. Sokolowska, E. Kurowska, P. Faller, *Biochim. Biophys. Acta, Gen. Subj.* **2013**, 1830, 5444-5455.
- [2] M. Fasano, S. Curry, E. Terreno, M. Galliano, G. Fanali, P. Narciso, S. Notari, P. Ascenzi, *IUBMB Life* **2005**, 57, 787-796.

- [3] K. B. Handing, I. G. Shabalin, O. Kassar, S. Khazaipoul, C. A. Blindauer, A. J. Stewart, M. Chruszcz, W. Minor, *Chem. Sci.* **2016**, *7*, 6635-6648.
- [4] C. Harford, B. Sarkar, *Acc. Chem. Res.* **1997**, *30*, 123-130.
- [5] A. J. Stewart, C. A. Blindauer, S. Berezenko, D. Sleep, P. J. Sadler, *Proc. Natl. Acad. Sci. U. S. A.* **2003**, *100*, 3701-3706.
- [6] P. J. Sadler, J. H. Viles, *Inorg. Chem.* **1996**, *35*, 4490-4496.
- [7] W. Bal, J. Christodoulou, P. J. Sadler, A. Tucker, *J. Inorg. Biochem.* **1998**, *70*, 33-39.
- [8] E. O. Martins, T. Drakenberg, *Inorg. Chim. Acta* **1982**, *67*, 71-74.
- [9] E. Mothes, P. Faller, *Biochemistry* **2007**, *46*, 2267-2274.
- [10] M. Sokołowska, M. Wszelaka-Rylik, J. Poznański, W. Bal, *J. Inorg. Biochem.* **2009**, *103*, 1005-1013.
- [11] J. Christodoulou, P. J. Sadler, A. Tucker, *Eur. J. Biochem.* **1994**, *225*, 363-368.
- [12] A. I. Ivanov, J. Christodoulou, J. A. Parkinson, K. J. Barnham, A. Tucker, J. Woodrow, P. J. Sadler, *J. Biol. Chem.* **1998**, *273*, 14721-14730.
- [13] B. P. Espósito, R. Najjar, *Coord. Chem. Rev.* **2002**, *232*, 137-149.
- [14] J. P. C. Coverdale, J. P. Barnett, A. H. Adamu, E. J. Griffiths, A. J. Stewart, C. A. Blindauer, *Metalomics* **2019**, *11*, 1805-1819.
- [15] S. Al-Harhi, J. I. Lachowicz, M. E. Nowakowski, M. Jaremko, Ł. Jaremko, *J. Inorg. Biochem.* **2019**, *198*, 110716.
- [16] a) J. Costa Pessoa, S. Etcheverry, D. Gambino, *Coord. Chem. Rev.* **2015**, *301-302*, 24-48; b) E. Kioseoglou, S. Petanidis, C. Gabriel, A. Salifoglou, *Coord. Chem. Rev.* **2015**, *301-302*, 87-105; c) D. Rehder, *Future Med. Chem.* **2016**, *8*, 325-338; d) I. E. Leon, J. F. Cadavid-Vargas, A. L. Di Virgilio, S. B. Etcheverry, *Curr. Med. Chem.* **2017**, *24*, 112-148; e) D. Crans, C. L. Yang, A. Haase, X. Yang in *Metallo-Drugs: Development and Action of Anticancer Agents*, Vol. 18 (Eds.: A. Sigel, H. Sigel, E. Freisinger, R. K. O. Sigel), De Gruyter GmbH, Berlin, **2018**, pp. 251-280; f) D. Rehder, *ChemTexts* **2018**, *4*, 20; g) D. C. Crans, L. Henry, G. Cardiff, B. I. Posner in *Essential Metals in Medicine: Therapeutic Use and Toxicity of Metal Ions in the Clinic*, Vol. 19 (Eds.: P. L. Carver), De Gruyter GmbH, Berlin, **2019**, pp. 203-230.
- [17] a) N. D. Chasteen, J. Francavilla, *J. Phys. Chem.* **1976**, *80*, 867-871; b) K. Fukui, H. Ohya-Nishiguchi, M. Nakai, H. Sakurai, H. Kamada, *FEBS Lett.* **1995**, *368*, 31-35; c) G. R. Willsky, A. B. Goldfine, P. J. Kostyniak, J. H. McNeill, L. Q. Yang, H. R. Khan, D. C. Crans, *J. Inorg. Biochem.* **2001**, *85*, 33-42; d) M. Purcell, J. F. Neault, H. Malonga, H. Arakawa, H. A. Tajmir-Riahi, *Can. J. Chem.* **2001**, *79*, 1415-1421; e) B. D. Liboiron, K. H. Thompson, G. R. Hanson, E. Lam, N. Aebischer, C. Orvig, *J. Am. Chem. Soc.* **2005**, *127*, 5104-5115; f) D. Sanna, E. Garribba, G. Micera, *J. Inorg. Biochem.* **2009**, *103*, 648-655; g) D. Sanna, G. Micera, E. Garribba, *Inorg. Chem.* **2009**, *48*, 5747-5757; h) D. Sanna, P. Buglyo, G. Micera, E. Garribba, *J. Biol. Inorg. Chem.* **2010**, *15*, 825-839; i) E. Cobbinna, S. Mehtab, I. Correia, G. Gonçalves, I. Tomaz, I. Cavaco, T. Jakusch, E. Enyedi, T. Kiss, J. Costa Pessoa, *J. Mex. Chem. Soc.* **2013**, *57*, 180-191.
- [18] J. Costa Pessoa, E. Garribba, M. F. A. Santos, T. Santos-Silva, *Coord. Chem. Rev.* **2015**, *301-302*, 49-86.
- [19] I. Correia, T. Jakusch, E. Cobbinna, S. Mehtab, I. Tomaz, N. V. Nagy, A. Rockenbauer, J. Costa Pessoa, T. Kiss, *Dalton Trans.* **2012**, *41*, 6477-6487.
- [20] a) D. N. Chasteen in *Biological Magnetic Resonance*, Vol. 3 (Eds.: L. J. J. Berliner, J. Reuben), Plenum Press, New York, **1981**, pp. 53-119; b) T. S. Smith II, R. LoBrutto, V. L. Pecoraro, *Coord. Chem. Rev.* **2002**, *228*, 1-18.
- [21] a) B. D. Liboiron in *High Resolution EPR: Applications to Metalloenzymes and Metals in Medicine*, Vol. 28 (Eds.: L. Berliner, G. Hanson), Springer, New York, **2009**, pp. 507-549; b) S. C. Larsen, N. D. Chasteen in *Metals in Biology: Applications of High-Resolution EPR to Metalloenzymes*, Vol. 29 (Eds.: G. Hanson, L. Berliner), Springer, New York, **2010**, pp. 371-409.
- [22] a) F. Neese, *JBIC Journal of Biological Inorganic Chemistry* **2006**, *11*, 702-711; b) F. Neese, *Coord. Chem. Rev.* **2009**, *253*, 526-563; c) M. Medhavi, V. Ambarish Sharan, Shankaracharya, *Curr. Bioinf.* **2011**, *6*, 444-449; d) S. F. Sousa, A. J. M. Ribeiro, J. T. S. Coimbra, R. P. P. Neves, S. A. Martins, N. S. H. N. Moorthy, P. A. Fernandes, M. J. Ramos, *Curr. Med. Chem.* **2013**, *20*, 2296-2314; e) I. A. Guedes, C. S. de Magalhães, L. E. Dardenne, *Biophys. Rev.* **2014**, *6*, 75-87; f) P. Chaskar, V. Zoete, U. F. Röhrig, *J. Chem. Inf. Model.* **2014**, *54*, 3137-3152; g) P. Vidossich, A. Magistrato, *Biomolecules* **2014**, *4*, 616-645; h) P. Li, L. F. Song, K. M. Merz, *J. Phys. Chem. B* **2015**, *119*, 883-895; i) V. Muñoz Robles, E. Ortega-Carrasco, L. Alonso-Cotchico, J. Rodríguez-Guerra, A. Lledós, J.-D. Maréchal, *ACS Catalysis* **2015**, *5*, 2469-2480; j) Z. Wang, H. Sun, X. Yao, D. Li, L. Xu, Y. Li, S. Tian, T. Hou, *Phys. Chem. Chem. Phys.* **2016**, *18*, 12964-12975; k) M. Akhter, *JSM Chem.* **2016**, *4*, 1025; l) S. Agarwal, R. Mehrotra, *JSM Chem.* **2016**, *4*, 1024; m) N. S. Pagadala, K. Syed, J. Tuszynski, *Biophys. Rev.* **2017**, *9*, 91-102; n) Gunseli B. Akcapinar, Osman U. Sezerman, *Biosci. Rep.* **2017**, *37*; o) P. Li, K. M. Merz, *Chem. Rev.* **2017**, *117*, 1564-1686; p) L. Riccardi, V. Genna, M. De Vivo, *Nature Reviews Chemistry* **2018**, *2*, 100-112; q) L. Alonso-Cotchico, J. Rodríguez-Guerra, A. Lledós, J.-D. Maréchal, *Acc. Chem. Res.* **2020**, *53*, 896-905.
- [23] *WINEPR SimFonia*, version 1.25, Bruker Analytische Messtechnik GmbH, Karlsruhe, **1996**.
- [24] D. Sanna, G. Micera, E. Garribba, *Inorg. Chem.* **2010**, *49*, 174-187.
- [25] G. Sciortino, E. Garribba, J. R. G. Pedregal, J. D. Marechal, *ACS Omega* **2019**, *4*, 3726-3731.
- [26] a) G. Sciortino, J. Rodríguez-Guerra Pedregal, A. Lledós, E. Garribba, J.-D. Maréchal, *J. Comput. Chem.* **2018**, *39*, 42-51; b) G. Sciortino, E. Garribba, J.-D. Maréchal, *Inorg. Chem.* **2019**, *58*, 294-306.
- [27] P. E. M. Siegbahn, F. Himo, *Wiley Interdiscip. Rev. Comput. Mol. Sci.* **2011**, *1*, 323-336.

- [28] L. F. Vilas Boas, J. Costa Pessoa in *Comprehensive Coordination Chemistry*, Vol. 3 (Eds.: G. Wilkinson, R. D. Gillard, J. A. McCleverty), Pergamon Press, Oxford, **1985**, pp. 453-583.
- [29] R. J. DeKoch, D. J. West, J. C. Cannon, N. D. Chasteen, *Biochemistry* **1974**, *13*, 4347-4354.
- [30] a) M. L. Munzarová, M. Kaupp, *J. Phys. Chem. B* **2001**, *105*, 12644-12652; b) F. Neese, *J. Chem. Phys.* **2003**, *118*, 3939-3948; c) A. C. Saladino, S. C. Larsen, *J. Phys. Chem. A* **2003**, *107*, 1872-1878; d) A. C. Saladino, S. C. Larsen, *Catal. Today* **2005**, *105*, 122-133; e) C. P. Aznar, Y. Deligiannakis, E. J. Tolis, T. Kabanos, M. Brynda, R. D. Britt, *J. Phys. Chem. A* **2004**, *108*, 4310-4321.
- [31] a) G. Micera, E. Garribba, *J. Comput. Chem.* **2011**, *32*, 2822-2835; b) D. Sanna, G. Sciortino, V. Ugone, G. Micera, E. Garribba, *Inorg. Chem.* **2016**, *55*, 7373-7387.
- [32] E. Garribba, E. Lodyga-Chruscinska, G. Micera, A. Panzanelli, D. Sanna, *Eur. J. Inorg. Chem.* **2005**, 1369-1382.
- [33] E. Garribba, G. Micera, E. Lodyga-Chruscinska, D. Sanna, G. Sanna, *Eur. J. Inorg. Chem.* **2005**, 4953-4963.
- [34] J. R. Simard, P. A. Zunszain, J. A. Hamilton, S. Curry, *J. Mol. Biol.* **2006**, *361*, 336-351.
- [35] a) A. A. Bhattacharya, T. Grüne, S. Curry, *J. Mol. Biol.* **2000**, *303*, 721-732; b) S. Curry, P. Brick, N. P. Franks, *Biochimica et Biophysica Acta (BBA) - Molecular and Cell Biology of Lipids* **1999**, *1441*, 131-140.
- [36] a) J. Lu, A. J. Stewart, P. J. Sadler, T. J. T. Pinheiro, C. A. Blindauer, *Biochem. Soc. Trans.* **2008**, *36*, 1317-1321; b) C. A. Blindauer, I. Harvey, K. E. Bunyan, A. J. Stewart, D. Sleep, D. J. Harrison, S. Berezenko, P. J. Sadler, *J. Biol. Chem.* **2009**, *284*, 23116-23124; c) J. P. Barnett, C. A. Blindauer, O. Kassar, S. Khazaipoul, E. M. Martin, P. J. Sadler, A. J. Stewart, *Biochimica et Biophysica Acta (BBA) - General Subjects* **2013**, *1830*, 5456-5464; d) J. P. C. Coverdale, S. Khazaipoul, S. Arya, A. J. Stewart, C. A. Blindauer, *Biochimica et Biophysica Acta (BBA) - Molecular and Cell Biology of Lipids* **2019**, *1864*, 532-542.
- [37] a) D. De Mel, C. Suphioglu, *Nutrients* **2014**, *6*, 3245-3258; b) D. C. Bode, H. F. Stanyon, T. Hirani, M. D. Baker, J. Nield, J. H. Viles, *J. Mol. Biol.* **2018**, *430*, 919-934; c) O. Kassar, U. Schwarz-Linek, C. A. Blindauer, A. J. Stewart, *Journal of Thrombosis and Haemostasis* **2015**, *13*, 101-110; d) J. Jansen, W. Karges, L. Rink, *The Journal of Nutritional Biochemistry* **2009**, *20*, 399-417; e) M. Soinio, J. Marniemi, M. Laakso, K. Pyörälä, S. Lehto, T. Rönnemaa, *Diabetes Care* **2007**, *30*, 523-528.
- [38] G. V. Richieri, A. M. Kleinfeld, *J. Lipid Res.* **1995**, *36*, 229-240.
- [39] a) A. P. Ginsberg, *J. Am. Chem. Soc.* **1980**, *102*, 111-117; b) L. Noodleman, *J. Chem. Phys.* **1981**, *74*, 5737-5743.
- [40] T. D. Smith, J. R. Pilbrow, *Coord. Chem. Rev.* **1974**, *13*, 173-278.
- [41] S. S. Eaton, K. M. More, B. M. Sawant, G. R. Eaton, *J. Am. Chem. Soc.* **1983**, *105*, 6560-6567.
- [42] M. Yoshizawa, K. Ono, K. Kumazawa, T. Kato, M. Fujita, *J. Am. Chem. Soc.* **2005**, *127*, 10800-10801.
- [43] M. J. Frisch, G. W. Trucks, H. B. Schlegel, G. E. Scuseria, M. A. Robb, J. R. Cheeseman, G. Scalmani, V. Barone, B. Mennucci, G. A. Petersson, H. Nakatsuji, M. L. Caricato, X., H. P. Hratchian, A. F. Izmaylov, J. Bloino, G. Zheng, J. L. Sonnenberg, M. Hada, M. Ehara, K. Toyota, R. Fukuda, J. Hasegawa, M. Ishida, T. Nakajima, Y. Honda, O. Kitao, H. Nakai, T. Vreven, J. A. Montgomery, Jr., J. E. Peralta, F. Ogliaro, M. Bearpark, J. J. Heyd, E. Brothers, K. N. Kudin, V. N. Staroverov, T. Keith, R. Kobayashi, J. Normand, K. Raghavachari, A. Rendell, J. C. Burant, S. S. Iyengar, J. Tomasi, M. Cossi, N. Rega, J. M. Millam, M. Klene, J. E. Knox, J. B. Cross, V. Bakken, C. J. Adamo, J., R. Gomperts, R. E. Stratmann, O. Yazyev, A. J. Austin, R. Cammi, C. Pomelli, J. W. Ochterski, R. L. Martin, K. Morokuma, V. G. Zakrzewski, G. A. Voth, P. Salvador, J. J. Dannenberg, S. Dapprich, A. D. Daniels, Ö. Farkas, J. B. Foresman, J. V. Ortiz, J. Cioslowski, D. J. Fox, *Gaussian 09, revision D.01*, Gaussian, Inc., Wallingford, CT, **2010**.
- [44] A. V. Marenich, C. J. Cramer, D. G. Truhlar, *J. Phys. Chem. B* **2009**, *113*, 6378-6396.
- [45] A. Šali, T. L. Blundell, *J. Mol. Biol.* **1993**, *234*, 779-815.
- [46] D. A. Case, R. M. Betz, D. S. Cerutti, T. E. Cheatham III, T. A. Darden, R. E. Duke, T. J. Giese, H. Gohlke, A. W. Goetz, N. Homeyer, S. Izadi, P. Janowski, J. Kaus, A. Kovalenko, T. S. Lee, S. LeGrand, P. Li, C. Lin, T. Luchko, R. Luo, B. Madej, D. Mermelstein, K. M. Merz, G. Monard, H. Nguyen, H. T. Nguyen, I. Omelyan, A. Onufriev, D. R. Roe, A. Roitberg, C. Sagui, C. L. Simmerling, W. M. Botello-Smith, J. Swails, R. C. Walker, J. Wang, R. M. Wolf, X. Wu, L. Xiao, P. A. Kollman, *AMBER 2016*, University of California, San Francisco, CA, **2016**.
- [47] V. Hornak, R. Abel, A. Okur, B. Strockbine, A. Roitberg, C. Simmerling, *Proteins: Struct., Funct., Bioinf.* **2006**, *65*, 712-725.
- [48] P. Li, K. M. Merz, *J. Chem. Inf. Model.* **2016**, *56*, 599-604.
- [49] P. Eastman, J. Swails, J. D. Chodera, R. T. McGibbon, Y. Zhao, K. A. Beauchamp, L.-P. Wang, A. C. Simmonett, M. P. Harrigan, C. D. Stern, R. P. Wiewiora, B. R. Brooks, V. S. Pande, *PLoS Comput. Biol.* **2017**, *13*, e1005659.
- [50] J. Rodríguez-Guerra Pedregal, L. Alonso-Cotchico, L. Velasco-Carneros, J.-D. Maréchal, *OMMProtocol: A Command Line Application to Launch Molecular Dynamics Simulations with OpenMM*, **2018**.
- [51] G. Jones, P. Willett, R. C. Glen, A. R. Leach, R. Taylor, *J. Mol. Biol.* **1997**, *267*, 727-748.
- [52] E. F. Pettersen, T. D. Goddard, C. C. Huang, G. S. Couch, D. M. Greenblatt, E. C. Meng, T. E. Ferrin, *J. Comput. Chem.* **2004**, *25*, 1605-1612.
- [53] a) G. Sciortino, D. Sanna, V. Ugone, G. Micera, A. Lledós, J.-D. Maréchal, E. Garribba, *Inorg. Chem.* **2017**, *56*, 12938-12951; b) G. Sciortino, D. Sanna, V. Ugone, A. Lledós, J.-D. Maréchal, E. Garribba, *Inorg. Chem.* **2018**, *57*, 4456-4469; c) G. Sciortino, D. Sanna, V. Ugone, J. D. Marechal, E. Garribba, *Inorg. Chem. Front.* **2019**, *6*, 1561-1578; d) G. Sciortino, D. Sanna, V. Ugone, J.-D. Maréchal, M. Alemany-Chavarria, E. Garribba, *New J. Chem.* **2019**, *43*, 17647-17660; e) V. Ugone, D. Sanna, G. Sciortino, J. D. Marechal, E. Garribba, *Inorg. Chem.* **2019**, *58*, 8064-8078.

- [54] S. C. Lovell, J. M. Word, J. S. Richardson, D. C. Richardson, *Proteins: Struct., Funct., Bioinf.* **2000**, *40*, 389-408.
- [55] a) J. Rodríguez-Guerra, *Insilichem/gauidiview: Pre-alpha public releas*, *Zenodo*, **2017**; b) J. Rodríguez-Guerra Pedregal, G. Sciortino, J. Guasp, M. Municoy, J.-D. Maréchal, *J. Comput. Chem.* **2017**, *38*, 2118-2126.
- [56] a) S. Gorelsky, G. Micera, E. Garribba, *Chem.–Eur. J.* **2010**, *16*, 8167-8180; b) D. Sanna, V. L. Pecoraro, G. Micera, E. Garribba, *J. Biol. Inorg. Chem.* **2012**, *17*, 773-790.
- [57] a) F. Neese, *ORCA – An Ab Initio, DFT and Semiempirical Program Package, Version 4.0*, Max-Planck-Institute for Chemical Energy Conversion, Mülheim a. d. Ruhr, **2017**; b) F. Neese, *Wiley Interdiscip. Rev. Comput. Mol. Sci.* **2017**, *8*, e1327.
- [58] E. Ruiz, J. Cano, S. Alvarez, P. Alemany, *J. Comput. Chem.* **1999**, *20*, 1391-1400.

Entry for the Table of Contents



An integrated approach based on spectroscopic and computational techniques was applied to unveil $V^{IV}O^{2+}$ binding modes to fatted and defatted human serum albumin. *N*-terminal (NTS) and multi-metal binding site (MBS) plus 'tertiary' (sites B) and 'quaternary' weak sites (sites C) were revealed. The influence of fatty acids in the formation of the adducts and the nature of the "strong" and "weak" sites were also explained.

WILEY-VCH